論文 / 著書情報
Article / Book Information

論題	
Title	Visualizing Carrier Motion in Organic Devices by Electric Field Induced Optical Second Harmonic Generation
著者	岩本 光正, 間中 孝彰, 田口 大
Author	Mitsumasa Iwamoto, Takaaki Manaka, Dai Taguchi
掲載誌/書名	, 2, , 17-28
Journal/Book name	Display and Imaging, 2, , 17-28
発行日 / Issue date	2015, 1
URL	http://www.oldcitypublishing.com/journals/display-and-imaging-home/display-and-imaging-issue-contents/d-i-volume-2-number-1-2015/
Note	このファイルは著者（最終）版です。 This file is author (final) version.

Visualizing carrier motion in organic devices by electric field induced optical second harmonic generation

Mitsumasa Iwamoto, Takaaki Manaka, and Dai Taguchi

Department of Physical Electronics, Tokyo Institute of Technology, 2-12-1 O-okayama, Meguro-ku, Tokyo 152-8552, Japan

By probing dielectric polarization originating from electric field arisen from carriers, we visualize carrier motions in organic devices. The method we use is electric field induced optical second harmonic generation (EFISHG) measurement, where nonlinear polarization induced in solids by coupling with incident electromagnetic waves of laser beam and dc electric field that is originating from moving carriers is visualized; Experiments making use of time-resolved EFISHG technique reveals carrier transfer in organic films. The authors anticipate that a novel technique using EFISHG can be a powerful tool to visualize carrier behaviors in organic devices.

Keywords: electric-field-induced optical second-harmonic generation, imaging system, nonlinear polarization, organic device, Maxwell-Wagner effect, electrical circuit analysis,

carrier motion, anisotropy, space charge field, interfacial charge propagation.

1. INTRODUCTION

Probing and modeling of carrier transport in materials is a fundamental research subject in electronics and materials science [1-3]. According to Maxwell's electromagnetic field theory [4], the Maxwell displacement current (MDC) is generated in a short circuit when the electric flux density originating from carriers changes with time [5]. Therefore, we can study dynamical carrier motion in solids, if change of the electric flux density is able to be probed [6]. Time-of-flight (TOF) technique [7] is often exerted to probing carrier transfer in solids sandwiched between two electrodes, to determine the carrier mobility. What we measure by using this TOF technique is the change of amount of induced charge on the electrode connected to an ammeter. Hence, the principle of the TOF measurement is basically probing the MDC. In the TOF, a long-range carrier motion in solids is recorded as a transient current, from which we can determine the transit time of carriers and thus estimate the carrier mobility [7-9]. However, the location of carriers traveling across organic materials cannot be determined. Also it is difficult to determine the polarity of carriers when we apply an e-TOF measurement, by replaying the general laser-TOF measurement with the e-TOF measurement. The way to overcome this situation is to directly probe the variation of the electric flux distribution that originate from carriers with time, not to probe change of charges induced on electrodes [10].

Time-resolved microscopic optical second harmonic generation (TRM-SHG) is a technique

that enables us to probe the propagation of the dielectric polarization induced by moving carriers, where nonlinear polarization induced in solids by coupling with incident laser beam and dc electric field generated from moving carriers is probed on-time [11]. Furthermore, using a charge-coupled device (CCD) imaging system directly visualizes their motion. Noteworthy we use incident laser beam to generate carriers in the laser-TOF measurement, while we use it to generate nonlinear polarization in the TRM-EFISHG measurement. This paper describes the technique to probe carrier motion in solids by using electric field induced optical second harmonic generation (EFISHG).

2. METHODS

The basic concept of the direct probing of carrier motions lies in the detection of non-zero dc field $E(0)$ arising from the carriers according to the Gauss law in the electro-magnetic theory, by detecting nonlinear polarization P which is freshly induced in solids by laser irradiation, owing to the interaction between electromagnetic field of laser beams and electrons in the solid molecules [12-14]. As an electron cloud of molecules is distorted by the presence of dc field, $E(0)$, this kind of nonlinear polarization P can be induced in all molecular systems, including symmetric molecular systems such as pentacene and phthalocyanine [13-15]. The induced nonlinear polarization is described as [10]

$$P(2\omega) = \chi^{(3)}(2\omega;0,\omega,\omega)E(0)E_i(\omega)E_j(\omega) \quad , \qquad (1)$$

where $\chi^{(3)}(2\omega;0,\omega,\omega)$ represents the nonlinear optical susceptibility of molecular systems, ω stands for the angular wave frequency of incident electromagnetic wave, $E_i(\omega)$ and $E_j(\omega)$ represent the electric fields of light, and $E(0)$ is the static electric field arising from moving-carriers, which satisfies the relation

$$\nabla \cdot \vec{E}(0) = \frac{en}{\varepsilon_s \varepsilon_0} \quad , \qquad (2)$$

where *n* is the carrier density, ε_s and ε_0 are, respectively, relative dielectric constant of molecular systems and dielectric constant of a vacuum.

As the induced polarization $P(2\omega)$ is a source of second harmonic signal, and results in the enhancement of electric field induced SH signal $I(2\omega)$ in proportion to the square of $P(2\omega)$, in a manner as

$$I(2\omega) \propto \left|P(2\omega)\right|^2 = \left|\chi^{(3)}(2\omega;0,\omega,\omega)E(0)E_i(\omega)E_j(\omega)\right|^2 . \qquad (3)$$

Here $I(2\omega)$ describes the SH intensity, and is called as the electric field induced optical second harmonic generation (EFISHG).

In electronic devices, there are many sources of d. c. electric fields. Among them are applying external voltages, moving carriers, trapped charges, work function difference and so forth

[16-22]. Consequently, the $E(0)$ in Eq. (3) is preplaced with Eq. (4) in a way as

$$E(0) = E_{ext}(0) + E_m(0) + E_t(0) + \cdots \quad , \tag{4}$$

where $E_{ext}(0)$, $E_m(0)$, and $E_t(0)$ represent electric files caused by applying external voltages, moving carriers, and trapped charges, respectively. Eq. (3) with Eq. (4) suggests that we can probe the carrier motion, by probing the change of electric field $E_m(0)$ in the time-resolved EFISHG measurement (TRM-EFISHG)

It is noteworthy that $\chi^{(3)}(0, \omega, \omega)$ is a material dependent parameter, and it specifies the feature of molecular systems. As a result, the SHG is activated at a specific wave length 2ω, depending on materials, and this fact allows us to selectively probe SHG generated from one of the layer of multi-layer systems by choosing incident laser wavelength appropriately [23-26]. Further as resonant enhancement of EFISHG occurs when the SH wavelength coincides with the absorption peak, generation of photo-carriers that possibly affect the electrical properties of devices can be neglected in the measurement, because the absorption of the fundamental light is negligible. Consequently, we can measure carrier transfer and so forth in a non-destructive way. In other words, we use laser irradiation to generate nonlinear polarization, and not to generate photo carriers.

3. EXPERIMENTAL SYSTEM

Figure 1a shows the basic arrangement of the experimental system used for the measurement of carrier transfer in organic semiconductor layer used as the organic field effect transistor (OFET) channel, where laser beam is vertically incident onto the top-contact OFET through the objective lens, and enhanced SHG images are captured with time by using a CCD camera [10,11]. The light source is an optical parametric oscillator (OPO), pumped by a third-harmonic light of Q-switched Nd-YAG laser (Continuum: SureliteII-10). To observe the SHG signal from the OFET, a fundamental wavelength is chosen, depending on the optical property of the semiconductor layer of the OFETs [23-26]. For example, it is chosen at 1120 nm for studying carrier transport in pentacene layer, whereas it is 820 nm for studying the carrier motion in α-NPD layer. SH light generated from the OFET is filtered by a fundamental-cut filter and an interference filter to remove fundamental and other unnecessary light. Figure 1b illustrates an example of timing chart of the laser pulse and voltage applied to the OFET, which is used for the time-resolved EFISHG measurement. The parameter τ stands for the delay time, and by choosing the delay time τ we can visualize carrier motions at time t = τ after applying the step voltage at t =0, and determine electric field distribution in OFETs using the visualized carrier images. At t = 0, just after applying the step voltage, carrier injection starts but still with

no carrier injection into OFETs, while at t = τ there are injected carriers along the channel of OFETs. That is, we can directly visualize electric field distribution formed by external voltages in organic devices by choosing τ =0, whereas we can map injected carrier distribution with time.

4. VISULALIZED CARRIER MOTION IMAGES

4.1 Carrier Transit in the Channel of OFETs

As mentioned in section 2, it is possible to probe carrier motion by means of the EFISHG. Using top-contact pentacene FETs with Au source and drain electrodes, time-resolved EFISHG measurement has been carried out [10,11]. Here the channel length of the OFET is 40 μm. Figure 2a shows the TRM-SHG image from the channel of pentacene FET with 500 nm-thick SiO_2 gate insulator, where the SHG image was obtained along with carrier motions after positive voltage pulse was applied to the Source electrode. That is, positive voltage pulse V_{pulse}=70 V was applied to the source electrode with respect to the gate and drain electrodes which were grounded, i.e., $V_{ds} = V_{gs} = -70$ V. At τ = 0 ns, the laser pulse coincides with the rising edge of the voltage pulse, and SHG signals are found near the edge of source electrode, indicating the Laplace electric field $E_{0,}$ parallel to the channel, is formed only around source electrode. Interestingly, as is clearly shown in the image, the emission band of the SHG signal

gradually moves in the channel from the source to drain electrode with elapsed time. The visualized emission band motion leaving from the source electrode for the drain electrode is the direct evidence of hole-injection from the Au-source electrode. That is, pentacene-FET shows a *p*-type behavior, where majority carriers are holes injected from the source electrode and the carrier mobility is estimated as 0.1–0.2 $cm^2\ V^{-1}\ s^{-1}$ from the visualized SHG images with time. Note that the SHG image is confined in the region within a radius of around 150 μm, because of the spot-size of laser (see the region indicated by dashed circle in Figure 2a. To further clarify the hole-transport mechanism across the channel, we plotted the SHG intensity profile, as shown in Figure 2b, where the results were obtained by re-plotting the maximum SHG intensity position, illustrated in Figure 2a, with elapsed time. From Figure 2a, it is clear that holes travel in the direction from the source Au electrode to the drain electrode, on satisfying the square root time dependence [27-29]. This time dependence reflects the interface charge propagation process, and well accounts for a RC circuit ladder model that is employed for analyzing transient carrier transport along the OFET channel [30-33]. In more detail, the carrier transport is governed by the interface charge accumulation process. Consequently, the transit time t_{tr} is proportion to

$$t_{tr} \approx \frac{L^2}{\mu(V_{gs} - V_{th} - \frac{V_{ds}}{2})} \quad . \qquad (5)$$

Here μ is carrier mobility, L is channel length, V_{gs} is the applied gate-source voltage, V_{th} is threshold voltage, and V_{ds} is applied drain-source voltage. Eq. (5) suggests that the carrier migrates into the channel region from the edge of source and drain electrodes, even in the case of $V_{ds} = 0$ [34-36]. This is nothing but the interface charge propagation process which is governed by the interface charge accumulation process and modeled by using a RC ladder-circuit model. Noteworthy that this square root time dependence is not a result due to the carrier diffusion process.

On the other hand, under the application of positive pulse voltage ($V_{gs} > 0$), the position of the SHG peak never moves; the SHG signals are concentrated around the edge of source electrode during the measurement [11, 37], suggesting that the electron injection is prohibited.

4.2 Visualized Anisotropic Carrier Transport

It is well-known that carrier transport strongly dependent on the film preparation condition, crystallinity of deposited films, and others. Accordingly anisotropic carrier transport is generated in deposited films. For example, carrier transport along the long-molecular axis

direction is different from the transport perpendicular to the long-molecular axis direction, and we anticipate this difference leads to anisotropic carrier transport in films deposited by dipping-method, spin-coated method and others. Nevertheless, there are still no reports on the visualized anisotropic carrier transport images of organic thin films. The TRM-EFISHG images displayed in Figure 2 have motivated us to visualize the anisotropic carrier transfer in organic thin films [38]. Figure 2 with Eq. (5) suggests that carriers migrate into the films from the edge of electrodes by only applying non-zero gate-source voltage V_{gs}. In this situation we can visualize carrier transits from the edge of electrodes in all directions by using round-shape electrode. Figure 3a shows the visualized SHG images by holes into pentacene films from the edge of the round shape electrode. Here the pentacene is evaporated homogeneously on the substrate. Accordingly, the spreading speed of holes from the electrode edge is the same for all directions of the prepared films. As a result, we can see the round shape image of injected holes around the Au electrode. On the other hand, Figure 3b shows the visualized SHG images by holes into Poly[(9,9-dioctylfluorenyl-2,7-diyl)-co-bithiophene]) (F8T2)-films from the edge of the round shape electrode. Here the F8T2 films were prepared using the FTM method. As a result, anisotropic morphology is induced on the F8T2 film along the FTM direction. As we can see in the Figure 3b, the spreading speed of holes from the edge of the round shape electrode is totally directional dependent on the film. That is, we can see the distorted SHG

image of injected holes around the Au edge of electrode. The spreading to the FTM direction, i.e., molecular long-axis direction, is the most. Figure 3 shows that we can visualize anisotropic carrier motions in thin films.

As has been visualized in the anisotropic carrier motions, the visualized carrier motion should be dependent on the film condition. In that situation it is interesting to show the difference of EFISHG images of transit carriers in semiconductor films deposited on different substrates, e.g., pentacene films deposited on SiO_2 and pentacene films on PMMA gate insulators [29]. Figure 4 shows the result for the TRM-SHG experiments using samples with PMMA layer on the surface of gate insulator. Figures 4a and 4b show the results by applying pulse voltage $V_{gs} = V_{ds} = -70$ V. This condition is the same with the experiments shown in Figure 2 As seen in the experimental results, SHG intensity is concentrated in the front region of the propagating SHG profile. This result suggests that space-charge field $E_t(0)$ is formed along the OFET channel due to carrier trapping, along with the carrier transient. This situation is different from the carrier transits in pentacene films deposited on SiO_2 gate insulator, which is displayed in Figure 2, where the SHG images appear homogeneously along with hole carrier propagation. Difference in the carrier traps well account for the resulting visualized SHG images.

As mentioned above, EFISHG is available for visualizing carrier behaviors in organic thin films. Using this idea we can extend the technique to visualize carrier motions in a variety of devices, e.g., OFETs [39-41], OSCs [42-44], OLEDs [45-47], and so forth [48-50]. EFISHG has a potentiality to visualize carrier motions.

5. CONCLUSIONS

In this review paper, we summarized a novel method for visualizing carrier motions by using optical second harmonic generation, where nonlinear polarization induced in the presence of d. c. electric field is well probed by coupling with a laser beam. As carriers are source of electric field, we anticipate that this method is broadly available for visualizing carrier motions in devices, including inorganic devices.

REFERENCES

[1] Meier H. (1974). *Organic Semiconductors: Dark- and Photoconductivity of Organic Solids.* Weinheim: Verlag Chemie.

[2] Lampert M. A., Mark P. (1970). *Current Injection in Solids.* New York: Academic.

[3] Sessler G. M. (1980). *Electrets.* Berlin: Springer.

[4] Maxwell J. C. (1954). *A Treatise on Electricity and Magnetism* (3rd ed.). New York: Dover.

[5] Iwamoto M., Wu C. –X. (2001). *The Physical Properties of Organic Monolayers*. Singapore: World Scientific.

[6] Iwamoto M., Manaka T., Yamamoto T., Lim E. (2008). "Probing motion of electric dipoles and carriers in organic monolayers by Maxwell displacement current and optical second harmonic generation", *Thin Solid Films*, **517**, 1312.

[7] Kepler R. G. (1960). "Charge carrier production and mobility in anthracene crystals", *Phys. Rev.*, **119**, 1226.

[8] Weis M., Lin J., Manaka T., Iwamoto M. (2009). "Analysis of transient currents in organic field effect transistor: The time-of-flight method", *J. Phys. Chem. C*, **113**, 18459.

[9] Lin J., Weis M., Taguchi D., Manaka T., Iwamoto M. (2011). "Carrier propagation dependence on applied potentials in pentacene organic field effect transistors investigated by impedance spectroscopy and electrical time-of-flight techniques", *Jpn. J. Appl. Phys.*, **50**, 04DK01.

[10] (Invited Review Paper) Iwamoto M., Manaka T., Taguchi D. (2014). "Probing and modeling of carrier motion in organic devices by electric-field-induced optical second-harmonic generation", *Jpn. J. Appl. Phys.*, **53**, 100101.

[11] Manaka T., Lim E., Tamura R., Iwamoto M. (2007). "Direct imaging of carrier motion in

organic transistors by optical second-harmonic generation", *Nat. Photonics*, **1**, 581.

[12] Verbiest T., Clays K., Rodriguez V. (2009). *Second-order Nonlinear Optical Characterization Techniques: An Introduction*. New York: CRC.

[13] Shen Y. R. (1984). *The principles of Nonlinear Optics*. New York: John Wiley & Sons.

[14] Manaka T., Li C. Q., Cheng X. M., Iwamoto M. (2004). "Spectroscopic consideration of the surface potential built across phthalocyanine thin films on a metal electrode", *J. Chem. Phys.*, **120**, 7725.

[15] Li C.-Q., Manaka T., Cheng X.-M., Iwamoto M. (2003). "Study of second harmonic generation from copper-tetra-tert-butyl-phthalocyanine Langmüir-blodgett film/metal interface", *Jpn. J. Appl. Phys.*, **42**, 2516.

[16] Lim E., Taguchi D., Iwamoto M. (2013). "Study of rectifying property of ITO/PI/TIPS-pentacene/Au diodes by electric field induced optical second harmonic generation", *Org. Electron.*, **14**, 1903.

[17] Lim E., Taguchi D., Iwamoto M. (2011). "Probing charging effects induced in ITO/polyimide/6,13-Bis(triisopropylsilylethynyl)-pentacene/Au diodes by time-resolved optical second harmonic generation measurement", *Chem. Phys. Lett.*, **515**, 306.

[18] Lim E., Taguchi D., Iwamoto M. (2012). "Probing carrier behavior in organic semiconductor device by electric field induced optical second harmonic generation

measurement", *Org. Electron.*, **13**, 2489.

[19] Lim E., Taguchi D., Iwamoto M. (2013). "Probing electric field distribution change in ITO/PI/TIPS-pentacene/Au diodes by time-resolved optical second harmonic generation measurement", *Chem. Phys. Lett.*, **561-562**, 97.

[20] Zhang L., Taguchi D., Li J., Manaka T., Iwamoto M. (2010). "Probing of interfacial charging and discharging in double-layer devices with a polyimide blocking layer by time-resolved optical second harmonic generation", *J. Appl. Phys.*, **108**, 093707.

[21] Zhang L., Taguchi D., Manaka T., Iwamoto M. (2011). "Bulk-trap modulated Maxwell-Wagner type interfacial carrier relaxation process in a fullerene/polyimide double-layer device investigated by time-resolved second harmonic generation", *J. Appl. Phys.*, **110**, 033715.

[22] Cui X., Taguchi D., Manaka T., Iwamoto M. (2013). "Analysis of carrier behavior in C60/P(VDF-TrFE) double-layer capacitor by using electric-field-induced optical second-harmonic generation measurement", *J. Appl. Phys.*, **114**, 234504.

[23] Chen X., Taguchi D., Manaka T., Iwamoto M. (2014). "Selective observation of photo-induced electric fields inside different material components in bulk-heterojunction organic solar cell", *Appl. Phys. Lett.*, **104**, 013306.

[24] Shibata Y., Nakao M., Manaka T., Lim E., Iwamoto M. (2009). "Probing electric field distribution in underlayer of an organic double-layer system by optical second-harmonic

generation measurement", *Jpn. J. Appl. Phys.*, **48**, 021504.

[25] Zhang L., Taguchi D., Manaka T., Iwamoto M. (2011). "Direct probing of the selective electron and hole accumulation at organic/organic interfaces in a triple-layer organic device by time-resolved optical second harmonic generation", *Appl. Phys. Lett.*, **99**, 083301.

[26] Mashiko Y., Taguchi D., Weis M., Manaka T., Iwamoto M. (2012). "The Maxwell-Wagner model for charge transport in ambipolar organic field-effect transistors: The role of zero-potential position", *Appl. Phys. Lett.*, **101**, 243302.

[27] Manaka T., Liu F., Weis M., Iwamoto M. (2009). "Studying transient carrier behaviors in pentacene field effect transistors using visualized electric field migration", *J. Phys. Chem. C*, **113**, 10279.

[28] Manaka T., Liu F., Weis M., Iwamoto M. (2008). "Diffusionlike electric-field migration in the channel of organic field-effect transistors", *Phys. Rev. B*, **78**, 121302.

[29] Manaka T., Liu F., Weis M., Iwamoto M. (2010). "Influence of traps on transient electric field and mobility evaluation in organic field-effect transistors", *J. Appl. Phys.*, **107**, 43712.

[30] Lim E., Manaka T., Tamura R., Iwamoto M. (2006). "Maxwell-Wagner model analysis for the capacitance-voltage characteristics of pentacene field effect transistor", *Jpn. J. Appl. Phys.*, **45**, 3712.

[31] Weis M., Manaka T., Iwamoto M. (2009). "Origin of electric field distribution in organic

field-effect transistor: Experiment and analysis", *J. Appl. Phys.*, **105**, 024505.

[32] Weis M., Taguchi D., Manaka T., Iwamoto M. (2010). "Organic electronics: Relaxation time controlled devices", *Jpn. J. Appl. Phys.*, **49**, 04DK15.

[33] Weis M., Lin J., Taguchi D., Manaka T., Iwamoto M. (2010). "The charge transport in organic field-effect transistor as an interface charge propagation: The Maxwell-Wagner effect model and transmission line approximation", *Jpn. J. Appl. Phys.*, **49**, 071603.

[34] Manaka T., Lim E., Tamura R., Yamada D., Iwamoto M. (2006). "Probing of the electric field distribution in organic field effect transistor channel by microscopic second-harmonic generation", *Appl. Phys. Lett.*, **89**, 072113.

[35] Zhang L., Taguchi D., Masada H., Manaka T., Iwamoto M. (2012). "Channel formation as an interface charging process in a pentacene field effect transistor investigated by time-resolved second harmonic generation and impedance spectroscopy", *Jpn. J. Appl. Phys.*, **51**, 02BK08.

[36] Taguchi D., Masada H., Manaka T., Iwamoto M., Nishiura T., Iizuka T., Takemori T. (2012). "Probing a two-step channel formation process in injection-type pentacene field-effect transistors by time-resolved electric-field-induced optical second-harmonic generation measurement", *Org. Electron.*, **13**, 2801.

[37] Manaka T., Lim E., Tamura R., Iwamoto M. (2005). "Modulation in optical second

harmonic generation signal from channel of pentacene field effect transistors during device operation", *Appl. Phys. Lett.*, **87**, 222107.

[38] Manaka T., Matsubara K., Abe K., Iwamoto M. (2013). "Direct observation of anisotropic carrier transport in organic semiconductor by time-resolved microscopic optical second-harmonic imaging", *Appl. Phys. Express*, **6**, 101601.

[39] Weis M., Lin J., Taguchi D., Manaka T., Iwamoto M. (2010). "Insight into the contact resistance problem by direct probing of the potential drop in organic field-effect transistors", *Appl. Phys. Lett*., **97**, 263304.

[40] Yamada D., Manaka T., Lim E., Tamura R., Weis M., Iwamoto M. (2008). "Injected carrier distribution in a pentacene field effect transistor probed using optical second harmonic generation", *J. Appl. Phys.*, **104**, 074502.

[41] Mir I. A., Ahuja T., Kumar D., Taguchi D., Manaka T., Iwamoto M. (2010). "Carrier injection from polypyrrole coated gold electrode in pentacene field effect transistors", *Synth. Met.*, **160**, 2116.

[42] Chen X., Taguchi D., Manaka T., Iwamoto M. (2012). "Study of blocking effect of Cu-phthalocyanine layer in zinc oxide/pentacene/CuPc/C60/Al organic solar cells by electric field-induced optical second harmonic generation measurement", *Org. Electron.*, **14**, 320.

[43] Chen X., Taguchi D., Manaka T., Iwamoto M. (2014). "Study of multiple photovoltaic

processes in stacked organic active layers", *Org. Electron.*, **15**, 2014.

[44] Chen X., Taguchi D., Shino T., Manaka T., Iwamoto M. **(**2011). "Analysis of interface carrier accumulation and relaxation in pentacene/C60 double-layer organic solar cell by impedance spectroscopy and electric-field-induced optical second harmonic generation", *J. Appl. Phys.*, **110**, 074509.

[45] Sadakata A., Osada K., Taguchi D., Yamamoto T., Fukuzawa M., Manaka T., Iwamoto M. (2012). "Probing interfacial charge accumulation in ITO/α-NPD/Alq3/Al diodes under two electroluminescence operational modes by electric-field induced optical second-harmonic generation", *J. Appl. Phys.*, **112**, 083723.

[46] Taguchi D., Zhang L., Li J., Weis M., Manaka T., Iwamoto M. (2010). "Analysis of carrier transients in double-layer organic light emitting diodes by electric-field-induced second-harmonic generation measurement", *J. Phys. Chem. C*, **114**, 15136.

[47] Taguchi D., Nakamoto R., Manaka T., Iwamoto M. (2014). "Detection of pre-electrical breakdown of IZO/α-NPD/Alq3/Al light-emitting diodes by electric-field-induced optical second-harmonic generation measurement", *Jpn. J. Appl. Phys.*, **53**, 04EK02.

[48] Lee K., Weis M., Lin J., Taguchi D., Majková E., Manaka T., Iwamoto M. (2011). "Trapping effect of metal nanoparticle mono- and multilayer in the organic field-effect transistor", *J. Appl. Phys.*, **109**, 064512.

[49] Zhang L., Taguchi D., Li J., Manaka T., Iwamoto M. (2011). “Transport limited interfacial carrier relaxation in a double-layer device investigated by time-resolved second harmonic generation and impedance spectroscopy”, *Appl. Phys. Lett.*, **98**, 092109.

[50] Li J., Zhang L., Ou-Yang W., Taguchi D., Manaka T., Iwamoto M. (2010). “Study of carrier behavior in pentacene in a Au/pentacene/ferroelectric poly(vinylidene fluoride-trifluoroethylene)/indium tin oxide structure by electric-field-induced second-harmonic generation measurement”, *Jpn. J. Appl. Phys.*, **49**, 121601.

Figure Captions

Figure 1: (a) Optical setup of the experimental system used for the measurement of carrier transfer along the OFET channel and (b) example of timing chart of the laser pulse and voltage applied to the OFET.

Figure 2: Visualized carrier transport by the TRM-SHG. (a) Holes injected from the source electrode of the pentacene OFET ($V_{gs} = V_{ds}$ =-70 V). (b) The motion of maximum SHG intensity position with elapsed time. The plot exhibits the square root time dependence which originates electric field driven interfacial carrier propagation.

Figure 3: (a) TRM-SHG image of holes injected from the round shape electrode. (a) The vacuum-evaporated pentacene film. (b) The TIPS-pentacene film deposited by using FTM method, holes spreads along the FTM direction, uncovering the anisotropic film morphology of the F8T2 film.

Figure 4: SHG intensity distribution of pentacene-OFET with (a) SiO_2 and (b) PMMA insulator.

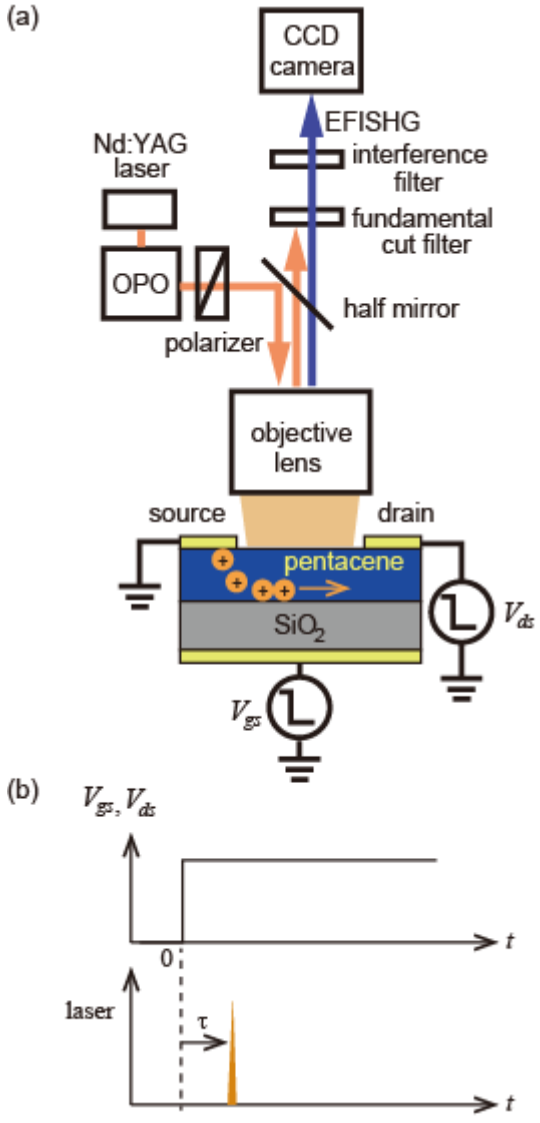

Figure 1: M. Iwamoto et al.

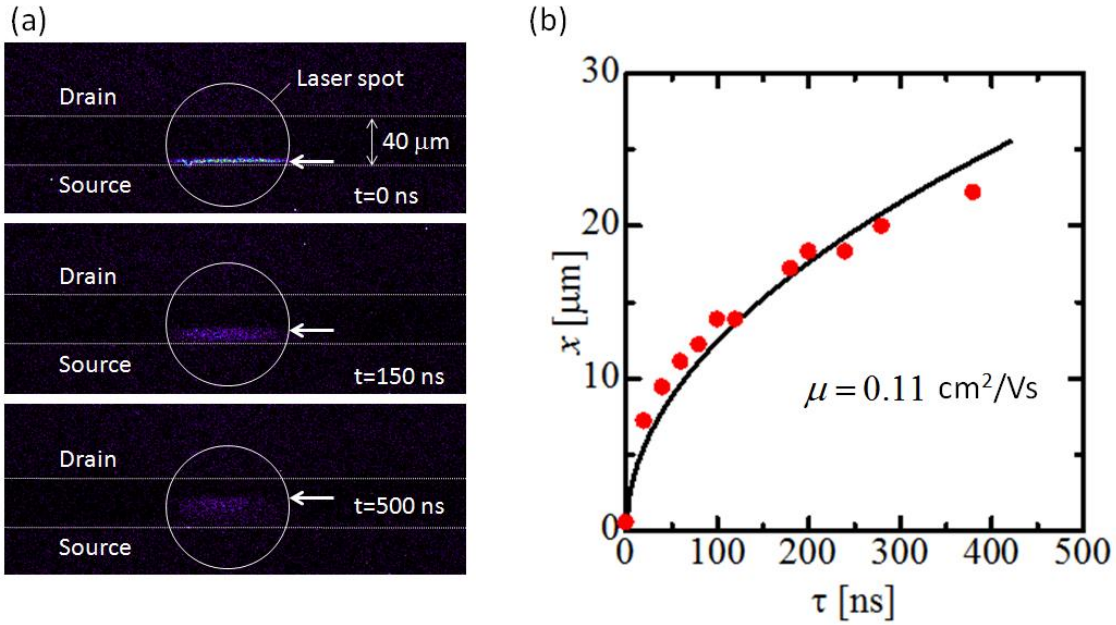

Figure 2: M. Iwamoto et al.

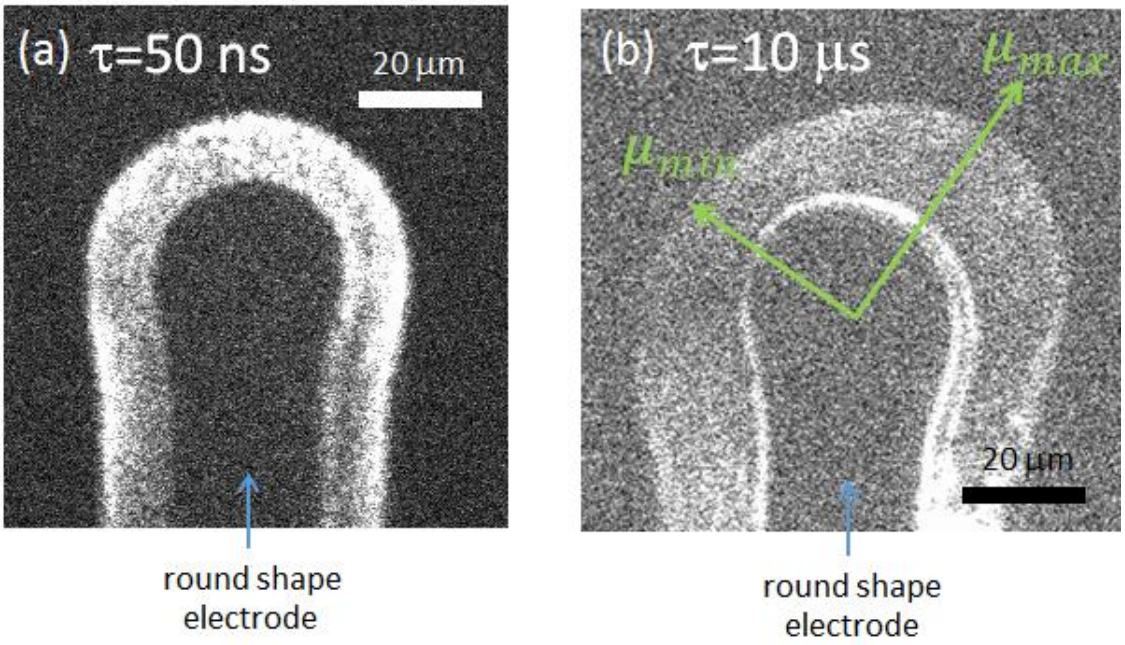

Figure 3: M. Iwamoto et al.

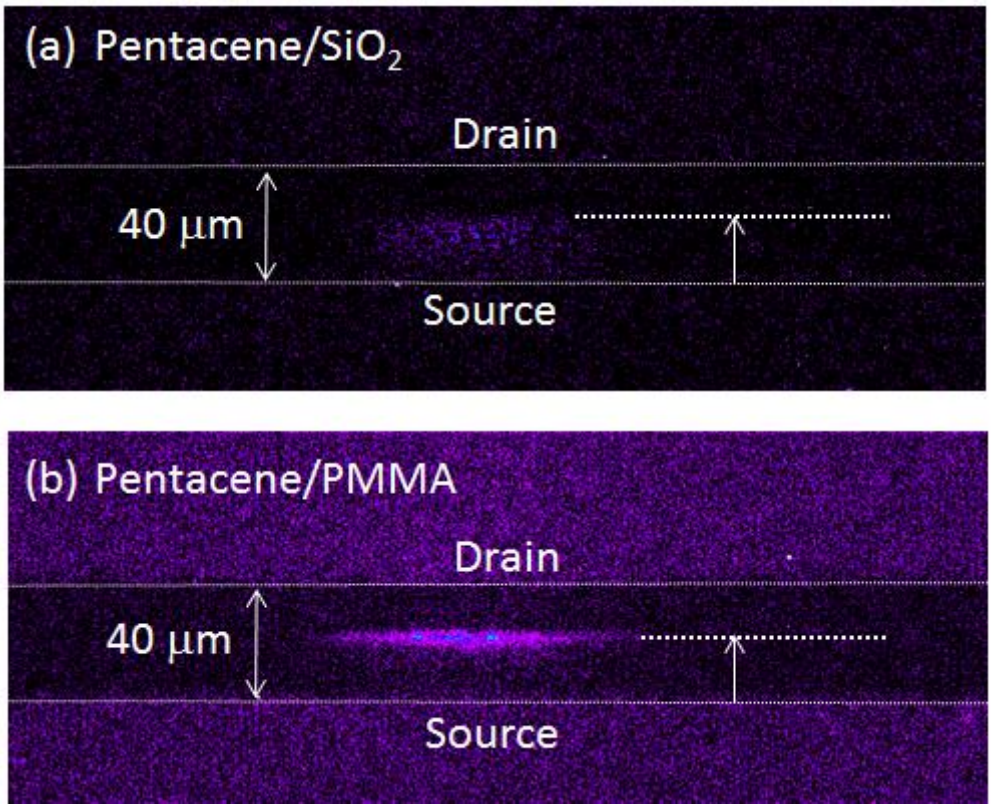

Figure 4: M. Iwamoto et al.